Reliability assessment of freight wagon passing through railway turnouts using adaptive Kriging surrogate model

Jun Lai [a, b, c], Kai Wang [a, b], Yan Shi [c,*], Jingmang Xu [a, b,*], Jiayin Chen [a, b], Ping Wang [a, b], Michael Beer [c, d, e]

[a] *MOE Key Laboratory of High-speed Railway Engineering, Southwest Jiaotong University, Chengdu 610031, China*

[b] *School of Civil Engineering, Southwest Jiaotong University, Chengdu, 610031, China*

[c] *Institute for Risk and Reliability, Leibniz Universität Hannover, Callinstr. 34, Hannover, 30167, Germany*

[d] *Institute for Risk and Uncertainty and School of Engineering, University of Liverpool, Peach Street, Liverpool L69 7ZF, UK*

[e] *International Joint Research Center for Resilient Infrastructure & International Joint Research Center for Engineering Reliability and Stochastic Mechanics, Tongji University, Shanghai 200092, China*

* Corresponding author's email address: rockousy@163.com (Yan Shi); mang080887@163.com (Jingmang Xu)

Abstract: Railway turnout (RT) is a crucial component of railway infrastructure that consists of several components. Assessing the derailment probability of freight wagons passing through the turnout is crucial for quantifying failure risks and optimizing the performance of the freight wagon-turnout system (FWTS). However, existing assessment methods often require extensive model evaluations and impose substantial computational costs. To address this issue, an efficient reliability analysis method is established for assessing the derailment risk at RTs. Firstly, a dynamic model is developed to capture the wheel-rail dynamic interaction and the numerical model is validated by field tests. Secondly, to reduce the computational cost in the reliability analysis, an efficient adaptive Kriging method based on an error stopping criteria and a learning function is adopted to estimate the failure probabilities under multiple failure modes of wheel derailments. Based on the efficient learning function and convergence criterion, accurate failure probability results can be obtained with a small number of multibody and finite element coupled dynamic simulations. Furthermore, the prediction accuracy of the proposed method in capturing random characteristics for FWTS is evaluated. Finally, the influence of the evolution of rail wear on the failure probability is further discussed.

Keywords: Railway turnouts; multibody dynamics; derailment risk; reliability analysis; adaptive Kriging model

1 Introduction

Railway turnouts play a crucial role in guiding trains from one track to another, enhancing the efficiency and flexibility of rail networks. Ensuring the safety and reliability of vehicle operations requires a thorough understanding of the uncertainty quantification (UQ) in the vehicle-turnout dynamic system, making it a subject of significant interest in academic research and engineering applications. When compared with the mainline, the dynamic interaction between the vehicle and turnout is more complicated. On the one hand, turnouts are constructed using multiple variable-section rails, resulting in discontinuous wheel-rail contact points. This discontinuity leads to high impact loads between the wheel and turnout [1]. On the other hand, sharp curves are widely set before or after the railway switch, increasing the likelihood of wheel flange contact. Shockingly, more than 30% of train derailments are related to the railway turnouts [2, 3]. Figure 1 illustrates a freight wagon derailment that occurred at a #1:6 symmetrical turnout in China. Based on field observations, the leading wheelset initially began climbing the rail from the switch toe and subsequently rolled a short distance on the railhead. Finally, the freight wagon drops down on the sleepers at the heel of the switch rail.

The long-term service of railway vehicles and turnout structures and high-density traffic loads would result in undesirable uncertainties, which in turn affects the dynamic interaction characteristics and safety of the freight wagon. These factors increase the derailment probabilities during railway vehicle passes through the RT, and increase the difficulty of random vibration analysis. For a comprehensive assessment and investigation of vehicle safety at RTs, it is crucial to carefully account for the uncertainties present in the FWTS.

Figure 1. A derailed freight wagon at a #1:6 turnout.

Some studies focus on the dynamic characteristics and passing performance during the railway vehicle

passes over the turnout. For instance, Kassa et al. [4] proposed a time-domain solution approach that addressed the general three-dimensional dynamic interaction between trains and turnouts (switches and crossings). Bruni et al. [5] compared different modelling approaches for the railway turnout system using finite element method (FEM) and multibody dynamics theory. Chang et al. [6] investigated the car-body shaking when high-speed train passes through the railway turnouts. Xu et al. [7] established an efficient method of time step variation to solve the matrix model for the vehicle-turnout model considering the multi-point contact between the wheel and turnout rails. In order to study the effect of high frequency vibration of the vehicle-turnout system, Chen et al. [8, 9] developed a refined vehicle-turnout dynamics algorithm called SDITT and investigated the effect of flexible deformation of the wheelset on the system vibrations. Lai et al [10, 11, 12] built a freight wagon-turnout coupled dynamic model to study the dynamic derailment under complex conditions.

However, the aforementioned studies did not account for uncertainties, which actually play a crucial role in understanding the dynamic behaviour of the FWTS comprehensively. Real-world scenarios involve uncertainties arising from manufacturing and assembly errors, variations in track geometries [13], train load variations, fluctuations in material properties, and degradation of vehicle suspension systems. Therefore, it is necessary to take this randomness into consideration, especially for complex track structures like turnouts.

Recent researches have increasingly focused on the uncertainties of vehicle-track (main line) and vehicle-track-bridge systems, primarily investigating stochastic vibration responses of the system [14]. Various methods, such as first/second order reliability method [15], Monte Carlo simulation (MCS) [16], response surface method (RSM) [17], probability density evolution method (PDEM) [18], and metamodel approach [19] have been used for reliability analysis of vehicle-track systems. For example, Li et al. [20] used RSM to assess the service reliability of high-speed trains considering the randomness of the wavelength of the track irregularities. Wang et al. [21] derived the stochastic equations of the vehicle-track dynamic model and predicted the random responses of the railway vehicle. Xu and Zhai [22] developed a comprehensive model for stochastic analysis and reliability assessment of vehicle-track systems subjected to random earthquakes and track irregularities.

Although the random finite element and multibody coupled dynamic simulation method can be employed to represent in vehicle and track parameters in the reliability analysis, they generally require a significant number of model evaluations and hence huge computational costs. To obtain accurate dynamic

response results, more complex structural models need to be constructed in the engineering practice. However, as the models become more refined, each numerical calculation can take several hours or longer, presenting challenges for structural reliability analysis and safety assessments under considering random parameters of freight wagon and RT. The conventional MCS method for uncertainty quantification has significant limitations due to its computational demands, especially for time-consuming numerical models in engineering problems. For cases with a low probability of failure, even more samples are required to ensure a desired level of accuracy. Unfortunately, for large-scale and complex nonlinear systems, the computational cost remains a challenge, limiting its practical implementation in real-world engineering problems. In order to reduce the computational effort, surrogate model based methods have attracted more focus for the reliability assessment of the large-scale mechanical systems and civil structures [23]. For example, Cremona et al. [24] combined Kriging technique and Archard wear model to predict the railway wheel considering the uncertainty of wear coefficient. Costa et al. [25] assessed the effect of track quality indices on the railway vehicle safety based on the surrogate model and multi-body dynamic simulation. In recent years, with the development of machine learning, the active learning Kriging surrogate method that combines with various active learning functions such as expected feasibility function (EFF) [26], U function [27, 28], and folded normal based expected improvement function (FNEIF) [29] has been proposed to improve the accuracy of the metamodel.

To the best of the authors' knowledge, there is no literature comprehensively addressing the reliability analysis and uncertainty quantification for the freight wagon-turnout system, particularly when considering multiple failure modes of wheel derailment, primarily due to the significant computational burden involved. To fill this apparent gap, this paper develops a research framework that uses an efficient adaptive Kriging surrogate and MCS method to study the reliability and the passing safety during freight wagon passing through railway turnouts. The research framework is shown in Figure 2. The initial samples are randomly selected in groups of 20. Then, the dynamic response results corresponding to the initial samples can be calculated by the freight wagon-turnout coupled dynamic model. They are used to construct the initial surrogate model. The candidate sample set is generated by MCS, which includes 5e05 random samples of the freight wagon-turnout system. Based on the initial surrogate model and candidate sample, the failure probability of train derailment can be calculated. Then, we need to determine the accuracy of the failure probability. If the computational accuracy is not enough, we need to select a new sample from the candidate

set based on active learning function and compute the vehicle-turnout dynamic response again, and then update the surrogate model. If the prediction accuracy of the derailment probability meets the thresholds, we can stop the loop.

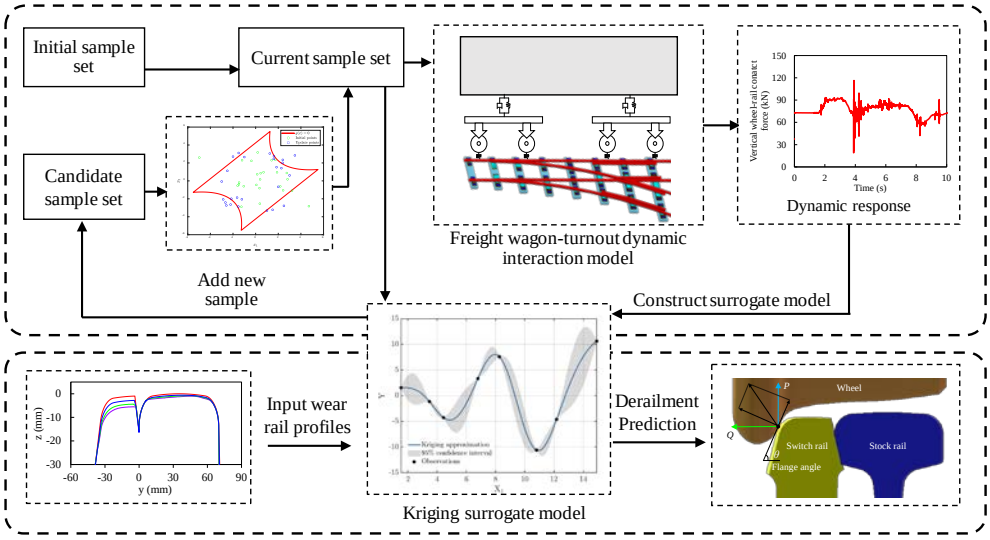

Figure 2. Research framework of adaptive dynamic reliability for a freight wagon-turnout system.

2 Model and formulation of a freight wagon-turnout system

2.1 Dynamic model of the freight wagon

A single freight wagon with two typical K6 type bogies is modelled as a multi-body system including the nonlinear elements, such as dry friction contact and wheel-turnout contact. The dynamic model and formulation of a freight wagon-turnout system created based on the framework of vehicle-track coupled dynamics theory [30]. The freight wagon sub-system is composed of one car-body, two bolsters, four side frames, and four wheelsets. For the bogie, the elastic rubber pads are installed on the wheelset axle box in actual condition. Non-linear spring elements are used to collect connect the wheelsets and side frames in the *X*, *Y*, and *Z* directions. Dry friction is commonly employed to model the frictional forces in the wheelset and axle box gap. Consequently, the dry friction force is discontinuous when the speed is 0, leading to numerical instability in the simulation. Therefore, a non-linear function had to be used to replace the lower sliding speed, with v_0 set to 0.01 m/s, as shown in Figure 3 (c), which is modelled as a nonlinear function in the dynamic model. The car-body of the freight wagon, depicted in Figure 3 (b), is supported by two bolsters connected through two center disks and four side bearings on the bolster. As shown in Figure 3 (d), the load on the bolster is transferred to the side frame through the secondary suspension spring. Friction wedges are

mounted on the side frame to achieve vibration attenuation. The degrees of freedom (DOFs) of each component of the freight wagon are listed in **Table 1**. The governing motion equation of the freight wagon model can be expressed as:

$$\mathbf{M}_{fw}\ddot{\mathbf{U}}_{fw}+\mathbf{C}_{fw}\dot{\mathbf{U}}_{fw}+\mathbf{K}_{fw}\mathbf{U}_{fw}=\mathbf{F}_{fw} \tag{1}$$

where $\mathbf{M}_{fw}$, $\mathbf{C}_{fw}$, $\mathbf{K}_{fw}$ are the mass matrix, damping matrix, and stiffness matrix of the freight wagon subsystem, respectively; $\ddot{\mathbf{U}}_{fw}$, $\dot{\mathbf{U}}_{fw}$, and $\mathbf{U}_{fw}$ are the displacement vector, velocity vector and acceleration vector of the freight wagon subsystem, respectively. $\mathbf{F}_{fw}$ is the vector of load such as the wheel-rail contact force (WRCF).

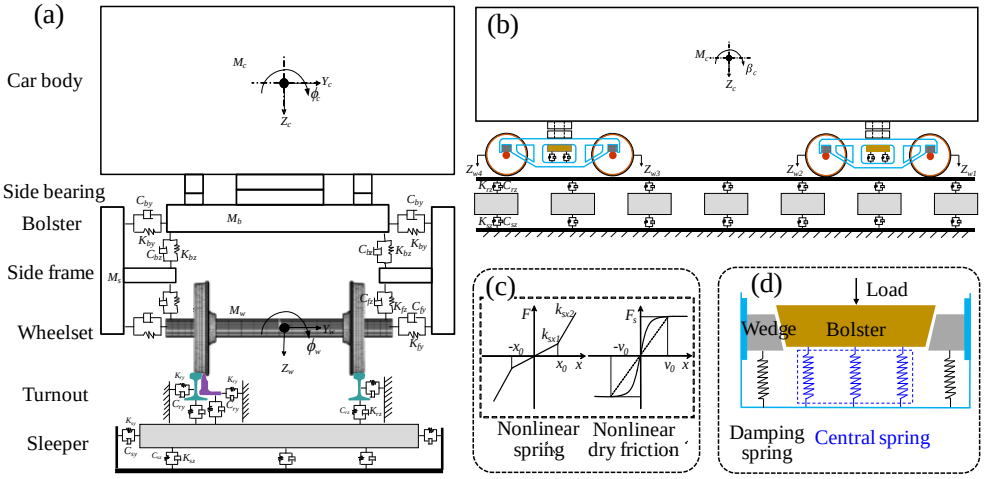

Figure 3. Diagram of dynamic model of freight wagon-turnout system. (a) front view, (b) side view, (c) modeling of the axle connection, and (d) variable friction damper model.

For the sake of brevity, the complete derivation process of the motion equations will be omitted here to conserve space. Interested readers are encouraged to refer to the work by Zhai [31] for detailed information. Furthermore, the deterministic parameters utilized in the freight wagon model for this paper are adopted from the work conducted by [31].

Table 1. DOFs of the freight wagon model.

Component	Type of motion					
	Longitudinal	Lateral	Vertical	Roll	Pitch	Yaw
Car-body	/	Y_c	Z_c	ϕ_c	β_c	φ_c
Side frame	X_s	Y_s	/	/	β_s	φ_s
Bolster	/	/	/	/	/	φ_b
Wheelset	/	Y_w	Z_w	ϕ_w	β_w	φ_w

2.2 Dynamic model of the turnout

Through field investigations of train derailments at railway turnouts, it has been observed that the

likelihood of derailments is notably high at 1:6 turnouts in China. As a result, this study focuses on modeling these specific turnouts. To maintain brevity, other turnout types are not considered in this paper. The geometry and alignment of the turnout are illustrated in Figure 4. The turnout configuration consists of a 2 m straight section, a 12 m curve, and a 40 m straight section preceding the switch toe.

To accurately represent the discrete support of the rails and account for any variations in rail properties, the turnout is modelled as a two-layer sub-system using the FEM. All rails in the turnout area are simulated using a point-supported Euler-Bernoulli beam element. Each rail node is assigned four DOFs, encompassing lateral, vertical, yaw, and pitch movements. The mathematical formulation for the Euler-Bernoulli beam element is elaborated in the work of Ref. [8]. The bending stiffness and mass of the switch rail vary along its length in accordance with the actual geometric and cross-sectional dimensions. The sleepers beneath the turnout rails are treated as discretely supported Euler beams in the vertical direction, allowing for flexibility. However, in the lateral direction, the sleepers are treated as rigid bodies. The turnout sleeper is discretized into different elements based on its length, and each sleeper node has two DOFs, accounting for vertical and roll movements.

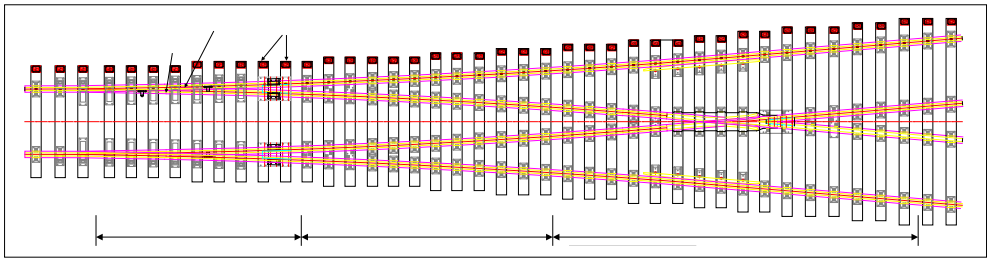

Figure 4. Geometry of the turnout structure.

By applying Hamilton's principle, the dynamic equation governing the turnout sub-system can be expressed as follows:

$$\int_{t1}^{t2}(\delta T-\delta U+\delta W)dt=0 \tag{2}$$

where T and U are the total kinetic energy and potential energy of the turnout system, respectively; W represents the virtual work done on the system by damping forces; t_1 and t_2 represent the start and end time of the integration.

The kinetic energy of the turnout sub-system is written as follows:

$$-\delta T=-(\sum_{j=1}^{N_r}\delta\mathbf{u}_{rj-z}^{T}\mathbf{M}_{rj}\ddot{\mathbf{u}}_{rj-z}+\sum_{j=1}^{N_r}\delta\mathbf{u}_{rj-y}^{T}\mathbf{M}_{rj}\ddot{\mathbf{u}}_{rj-y}+\sum_{j=1}^{N_s}\delta\mathbf{u}_{sj-z}^{T}\mathbf{M}_{sj}\ddot{\mathbf{u}}_{sj-z}+\sum_{j=1}^{N_s}\delta\mathbf{u}_{sj-y}^{T}\mathbf{M}_{sj}\ddot{\mathbf{u}}_{sj-y}) \tag{3}$$

in which N_r and N_s are the number of the rail elements and sleeper elements; $\mathbf{u}_{rj-z}^T$ and $\mathbf{u}_{rj-y}^T$ denote the displacement vectors of the rail elements in the vertical and lateral directions; $\mathbf{u}_{sj-z}^T$ and $\mathbf{u}_{sj-y}^T$ denote the displacement vectors of the sleeper elements in the vertical and lateral directions; $\mathbf{M}_{rj}$ and $\mathbf{M}_{sj}$ are the mass matrix of the rails and sleepers.

The potential energy of the turnout sub-system reads:

$$\begin{aligned}\delta U = &\sum_{j=1}^{N_r}\delta\mathbf{u}_{rj-z}^T\mathbf{K}_{rzj}\mathbf{u}_{rj-z}+\sum_{j=1}^{N_r}\delta\mathbf{u}_{rj-y}^T\mathbf{K}_{ryj}\mathbf{u}_{rj-y}+\sum_{j=1}^{N_s}\delta\mathbf{u}_{sj-z}^T\mathbf{K}_{sj-z}\mathbf{u}_{sj-z}\\ &+\sum_{j=1}^{N_f}[(\delta z_{rj}-\delta z_{sj})K_{fzj}(z_{rj}-z_{sj})+(\delta y_{rj}-\delta y_{sj})K_{fyj}(y_{rj}-y_{sj})+K_{f\beta j}\delta\beta_{rj}\ \cdot\ \beta_{rj}]\\ &+\sum_{j=1}^{N_p}\delta z_{sj}K_{bzj}z_{sj}+\sum_{j=1}^{N_m}\delta y_{sj}K_{byj}y_{sj}\end{aligned} \tag{4}$$

where $\mathbf{K}_{rzj}$ and $\mathbf{K}_{szj}$ are the stiffness matrices of elements of rails and sleepers in the vertical direction, respectively; $\mathbf{K}_{ryj}$ is the stiffness matrices of elements of rails in the lateral direction. where N_f represents the total number of the rail fasteners; N_p and N_m are the total number of sleeper nodes and number of sleepers, respectively; K_{rzj}, K_{ryj}, and $K_{r\beta j}$ are the vertical, lateral, and pitching stiffness of the j_{th} rail fastener, respectively; K_{szj} and K_{syj} are the vertical and lateral stiffness of the j_{th} sleeper; z_{rj}, y_{rj}, and β_{rj} are the vertical, lateral and pitch movements of the rail nodes, respectively; z_{sj} and y_{sj} are the vertical and lateral displacement of sleeper nodes, respectively.

The expression for the virtual work done by external loads is as follows:

$$\begin{aligned}\delta W = &\sum_{j=1}^{N_f}[C_{fj-z}(\delta z_{rj}-\delta z_{sj})(\dot{z}_{rj}-\dot{z}_{sj})+C_{fj-y}(\delta y_{rj}-\delta y_{sj})(\dot{y}_{rj}-\dot{y}_{sj})+K_{f\beta j}\delta\beta_{rj}\ \cdot\ \dot{\beta}_{rj}]\\ &+\sum_{j=1}^{N_p}C_{bj-z}\delta z_{si}\dot{z}_{si}+\sum_{j=1}^{N_m}C_{bj-y}\delta y_{si}\dot{y}_{si}\end{aligned} \tag{5}$$

where C_{fj-z} and C_{fj-y} are the vertical and lateral damping coefficients of the j_{th} rail fastener, respectively; C_{bj-z} and C_{bj-y} are the vertical and lateral damping coefficients of the j_{th} sleeper, respectively.

The dynamic equation of the turnout subsystem can be derived based on Equation (6):

$$\mathbf{M}_t\ddot{\mathbf{u}}_t+\mathbf{C}_t\dot{\mathbf{u}}_t+\mathbf{K}_t\mathbf{u}_t=\mathbf{F}_t \tag{6}$$

where $\mathbf{M}_r$, $\mathbf{K}_r$, and $\mathbf{C}_r$ are the mass, stiffness, and damping matrix of the railway turnout sub-system,

respectively; Where $\ddot{\mathbf{u}}_t$, $\dot{\mathbf{u}}_t$, and $\mathbf{u}_t$ represent the acceleration, velocity, and displacement vectors of the turnout sub-system, respectively; $\mathbf{F}_r$ denotes the load vector of contact forces between the wheel and the turnout rail.

2.3 Wheel-turnout contact model

When compared with straight track, the cross-sections of the switch rail and crossing rail are variable along with the longitudinal direction. Therefore, the 3D variable rail profiles are obtained by Bezier splines. For the ordinary track in front of the switch panel, contact trace method in Ref. [32] can be used to solve the contact position between the wheel and the rail. The contact trace indicating the potential contact positions on the left wheel profile can be obtained by

$$\begin{cases} x = x_{Oc} - l_x R_w \tan\delta_r \\ y = y_{Oc} + \dfrac{R_w}{1-l_x^{\,2}}(l_x^{\,2} l_y \tan\delta_r - l_z m) \\ z = z_{Oc} + \dfrac{R_w}{1-l_x^{\,2}}(l_x^{\,2} l_z \tan\delta_r - l_y m) \end{cases} \tag{7}$$

In which, $m = \sqrt{1-l_x^{\,2}(1+\tan^2\delta_r)}$, $\begin{cases} l_x = -\cos\theta_w \sin\varphi_w \\ l_y = \cos\theta_w \sin\varphi_w \\ l_z = \sin\theta_w \end{cases}$, $\begin{cases} x_{o2} = d_w l_x \\ y_{o2} = d_w l_y + y_w \\ z_{o2} = d_w + l_z \end{cases}$. R_w represents the wheel rolling radius; δ_r is the wheel-rail contact angle; θ_w and φ_w are the roll angle and yaw angle of the wheelset; y_w represents the lateral displacement of the wheelset; d_w represents the original y-coordinate vector of the wheel profile.

It should be noted that in case the wheel rolls from the stock rail to the switch rail, two-point contact case can occur at the wheel load transition zone, as show in Figure 5 C-C. An improved method is used to deal with this problem [7], the elastic compression between the wheel and turnout can be calculated by

$$\begin{cases} Q_{switch} = Z_w - (\tilde{Z}_{trc}^{wr} |_{\Phi switch} - Z_0) \\ Q_{stock} = Z_w - (\tilde{Z}_{trc}^{wr} |_{\Phi stock} - Z_0) \end{cases} \tag{8}$$

where Z_w represents the vertical displacement of the wheelset; $\tilde{Z}_{trc}^{wr}$ denotes minimum distance in the vertical direction between the wheel and rail; Z_0 is initial minimum distance in the vertical direction. When Q_{switch} is less than 0, it indicates that the wheel is in full contact with the stock rail; and when Q_{stock} is less than 0, the

wheel simultaneously contacts with the stock rail and switch rail; when both Q_{switch} and Q_{stock} are larger than 0, the wheel is in contact with both the stock rail and switch rail.

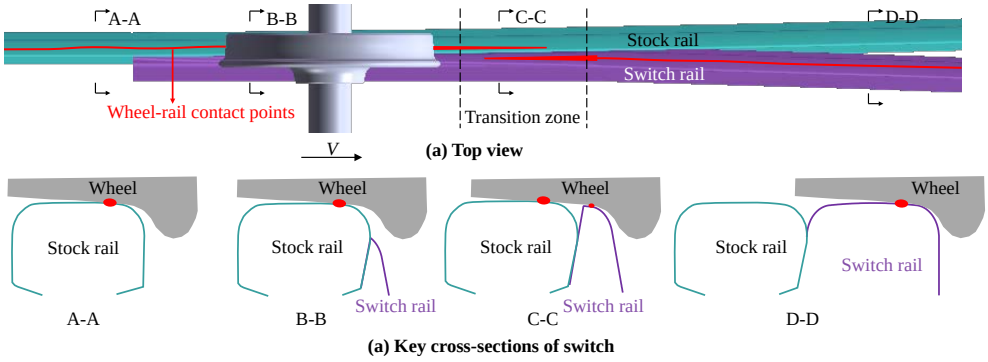

Figure 5. Wheel-turnout contact along with the railway switch.

The non-linear Hertz contact model and FASTSIM algorithm are used to solve the normal force, and tangential force between the wheel and rail, respectively. They consider various factors such as friction, adhesion, and wheel-rail contact geometry to accurately calculate the WRCF. The vibration equation is solved by the combination of the Newmark-β and Park methods. Based on the Newmark-β method, the vibration responses of the first three iterations of the system are obtained. Then, the vibration differential equation is solved by Park method.

2.4 Verification of freight wagon-turnout dynamic interaction model

The validation of the freight wagon-turnout coupled dynamic interaction model is conducted by comparing the vertical displacement of the turnout sleeper between the field test and numerical simulation. In the field test, a C70 type freight wagon with two three-piece bogies is used, and the running speed of the freight wagon is set to be 20 km/h with a wheelset axle load of 20.5 tons. The symmetrical railway turnout with a 1:6 crossing angle is used for both the test and the simulation. The displacement sensor in the test site measured the relative displacement between the rail base and sleeper. In addition, we affixed strain gauges to the rail web at the switch rail point to measure WRCFs. Assessing the derailment coefficient at the switch rail point is crucial for evaluating dynamic performance and ensuring operational safety. As such, we utilized the WRCFs acquired from the field test to calculate the derailment coefficient, which is determined by the ratio of lateral to vertical wheel/rail contact forces. To ensure the reliability of our verification, we collected ten sets of data, covering speed ranges from 16 km/h to 21 km/h.

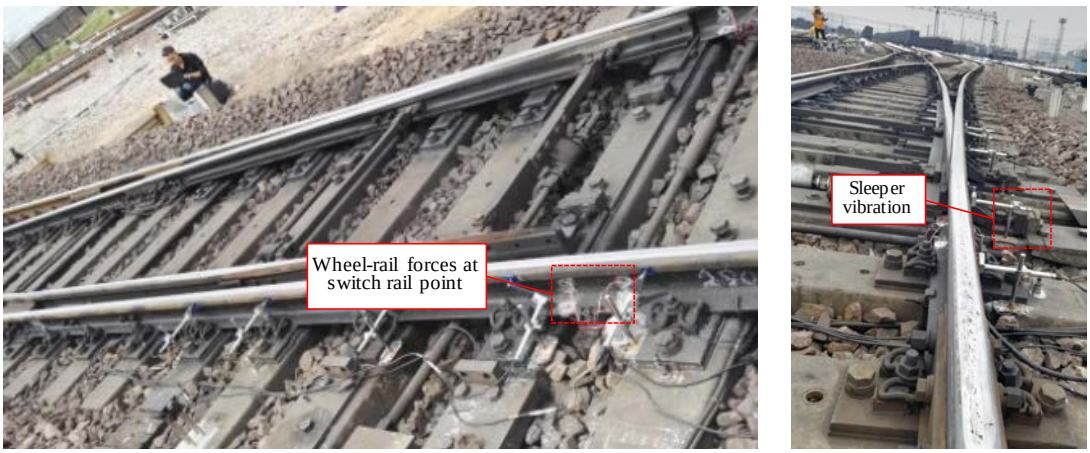

Figure 6. Field test for wheel-rail forces at switch rail point and sleeper vibration.

Figure 7(a) shows the comparison of displacement of turnout sleeper between the field test and numerical simulation. It can be observed that the change trend of test results is consistent with the simulation results. There is a slight difference between the numerical model and the test results in terms of amplitude of displacements. The maximum of the displacement obtained by experiment is 0.45 mm. Besides, as can be seen from Figure 7(b), we observe that the derailment coefficient calculated by our numerical simulation model closely align with the field test results. The slight discrepancy between the numerical results and the test results is because the randomness of parameters is not considered in the numerical model. This is because the vehicle parameters provided here are based on the design values. In reality, suspension parameters may change with the long-term operation of the vehicle. Additionally, the randomness of the wheel-rail friction coefficient can also affect the test results. In general, the numerical simulation results are found to be in good agreement with the field test results. This proves that the proposed numerical model is well suited for freight wagon-track (turnout) interactions.

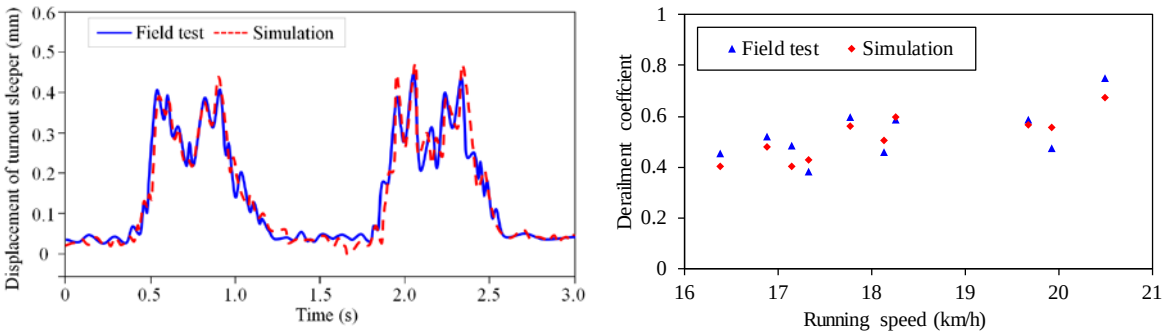

(a) (b)

Figure 7. Comparison between filed test and numerical simulation results: (a) Displacement of turnout sleeper, and (b) derailment coefficient at switch rail point.

3 Adaptive reliability analysis

3.1 Uncertainties in the freight wagon-turnout system

In the long-term service of railway infrastructure, the mechanical parameters of the FWTS result in the randomness of the WRCFs and wheelset vibrations. Therefore, it is crucial to study the propagation of uncertainties in the FWTS. Since the safety of the freight wagon primarily depends on the wheel-rail contact relationships, this paper focuses more on the dynamic responses of two typical derailment criteria, namely the derailment coefficient and the wheel load reduction rate (WLRR). The definition of the derailment coefficient is presented in Sec 2.4. The wheel load reduction rate is defined as $\Delta P / \overline{P}$, as shown in Equation (10).

Table 2. Random parameters of the freight wagon-turnout system.

Item	Random variable	Unit	Mean value	COV	Distribution type
1	Vehicle speed	km/h	17	0.05	Normal
2	Wheel-rail friction coefficient	/	0.4	0.1	Normal
3	Wheelset axle load	ton	15	0.1	Normal
4	Width of track gauge	mm	1435	1/1435	Normal
5	Lateral stiffness of secondary suspension	kN/m	2.5E03	0.1	Normal
6	Vertical stiffness of secondary suspension	kN/m	3.0E03	0.1	Normal
7	Height of mass center	m	1.4	0.05	Normal
8	Lateral deviation of center of gravity position	m	0	0.1	Normal
9	Longitudinal deviation of center of gravity position	m	0	0.4	Normal

The input parameters that significantly influence the wheel-rail contact, including vehicle speed, wheel-rail friction coefficient, wheelset axle load, rail gauge, suspension stiffness, and center of gravity position are considered as random variables. Since the focus of this study is on the validity and feasibility of using the adaptive Kriging surrogate model and ESC to deal with dynamic reliability of FWTS and derailment assessment, the random parameters are assumed to be normal distributions. The mean value and coefficient of variation (COV) for each random parameter are provided in Table 2.

3.2 Performance functions of FWTS

Reliability analysis for FWTS is to determine the probability of wheel derailment with considering uncertainties in system parameters. On the one hand, during the freight wagon enters the switch in an

unfavourable wheelset posture, a large impact may occur between the wheels and switch. The wheelset may jump up to the railhead of the switch. On the other hand, the small radius curves are widely set before and after the railway switch panel, resulting the large lateral wheel-rail force and further causing the wheels to climb up the railhead along the edge of the switch rail. Two primary failure modes of derailment exist: wheel climb derailment and wheel jump derailment. To assess these failure modes, the performance functions can be defined as follows:

$$g_1(\boldsymbol{\xi}) = \lambda - \frac{Q}{P} \tag{9}$$

$$g_2(\boldsymbol{\xi}) = \gamma - \frac{\Delta P}{\overline{P}} \tag{10}$$

$$g_3(\boldsymbol{\xi}) = \min\left\{\lambda - \frac{Q}{P},\ \gamma - \frac{\Delta P}{\overline{P}}\right\} \tag{11}$$

where Q, and P are the lateral and vertical WRCF, respectively; ΔP represents the value of wheel load loss and $\overline{P}$ is the average value of wheel loads P_2 and P_1 on two wheels; the value of wheel load loss is calculated by: $\Delta P=(P_2-P_1)/2$, $P_2>P_1$. $\boldsymbol{\xi}$ is the vector of random input parameters, as illustrated in Section 3.1; where λ and γ are the limit values of the derailment coefficient and WLRR, respectively.

The failure probability of wheel climb derailment is defined as:

$$P_{f1} = \text{Prob}\left[g_1(\xi) = \lambda - \frac{P}{Q} \le 0 \right] \tag{12}$$

The failure probability of wheel jump derailment is defined as:

$$P_{f2} = \text{Prob}\left[g_2(\xi) = \gamma - \frac{\Delta P}{\overline{P}} \le 0 \right] \tag{13}$$

The failure probability of both types of derailment is defined as:

$$P_{f3} = \text{Prob}\left[g_1(\xi) = \lambda - \frac{P}{Q} \le 0 \ \cup \ g_2(\xi) = \gamma - \frac{\Delta P}{\overline{P}} \le 0 \right] \tag{14}$$

where Prob represents the probability of failure; $\cup$ is the union of $g_1(\boldsymbol{\xi}) \le 0$ and $g_2(\boldsymbol{\xi}) \le 0$.

3.3 Adaptive Kriging model for reliability analysis of FWTS

The Kriging surrogate model technique provides a means of predicting the output values of a complex

system, which is a Gaussian process-based regression method. The Kriging model $g(\xi)$ can be expresses as

$$g(\xi) = f(\xi)\beta^T + Z(\xi) \tag{15}$$

In the Kriging model, $f(\xi)$ represents the basis function used for regression, and β^T denotes the vector of regression coefficients associated with the basis function $f(\xi)$; and $Z(\xi)$ is a stationary Gaussian process with zero mean and covariance between two points of space ξ_i and ξ_j, and the covariance is written as

$$cov(Z(\xi_i),\ Z(\xi_j)) = \sigma^2 R_\theta(\xi_i,\ \xi_j) \tag{16}$$

Where σ^2 is the process variance and $R_\theta(\xi_i,\ \xi_j)$ is the correlation function between two sample ξ_i and ξ_j. The Gaussian model is used in this study and it is expressed as in Eq. (17).

$$R_\theta(\xi_i,\ \xi_j) = \prod_{k=1}^{N} \exp\left(-\theta_k(\xi_{i,k} - \xi_{j,k})^2\right) \tag{17}$$

Where θ represent correlation coefficient; $\xi_{i,k}$ and $\xi_{i,k}$ are the denote the k_{th} of sample ξ_i and ξ_j.

The performance functions $g_1(\boldsymbol{\xi})$, $g_2(\boldsymbol{\xi})$ and $g_3(\boldsymbol{\xi})$ are implicit and strongly nonlinear between the input variables ξ and vibration response results $g(\xi)$. An accurate and efficient active learning Kriging model is integrated with theoretical model in Section 2 to train an initial Kriging surrogate model with small sample sets. In this paper, U learning function [27], known for its high efficiency, is utilized to update the training points for the rough surrogate model. The predicted mean $\hat{g}(\boldsymbol{\xi}_k)$ and variance $\hat{\sigma}(\boldsymbol{\xi}_k)$ of performance functions $g_1(\boldsymbol{\xi})$, $g_2(\boldsymbol{\xi})$, and $g_3(\boldsymbol{\xi})$ are utilized to represent the response and uncertainty, respectively. Its form is defined as follows:

$$U(\boldsymbol{\xi}_k) = \frac{\left|\hat{g}(\boldsymbol{\xi}_k)\right|}{\hat{\sigma}(\boldsymbol{\xi}_k)} \tag{18}$$

In general, the stopping criteria for the U learning function is set as $U(\boldsymbol{\xi}_k) \geq 2$ during the construction of the final Kriging prediction model. However, the stopping criterion in the adaptive process is intentionally set to be overly conservative because the variable U does not directly reflect the error in the estimated failure probability of wheel derailment at each iteration. This conservative approach aims to ensure that the true error in the failure probability estimate remains within an acceptable range. Despite the significant reduction in computation time achieved by the adaptive Kriging method for reliability analysis of the nonlinear dynamic system, the U function still requires a large number of iterations for numerical computation. To

address this limitation, an ESC is given in the next section to overcome this limitation [33].

In the real case, the true failure probability for the FWTS is unknown. Therefore, the failure probability P_f^{MCS} that is estimated by MCS can be used as the benchmark for measuring the accuracy. The prediction failure probability by adaptive Kriging surrogate model is $\hat{P}_f^{MCS}$. Let's establish the definitions for the actual failure probabilities and the predicted failure probabilities as follows:

$$P_f^{MCS} = \frac{N_f}{N_{MCS}} \tag{19}$$

$$\hat{P}_f^{MCS} = \frac{\hat{N}_f}{N_{MCS}} \tag{20}$$

in which N_f and $\hat{N}_f$ are the number of system failures determined by true performance function, and adaptive reliability assessment method, respectively; and N_{MCS} represents the candidate samples for MCS.

The relative error can be expresses as:

$$\varepsilon = \left| \frac{\hat{P}_f^{MCS}}{P_f^{MCS}} - 1 \right| = \left| \frac{\hat{N}_f}{N_f} - 1 \right| \tag{21}$$

Due to the unknown number of failures N_f, the true error ε in Kriging surrogate model cannot be determined. To deal with this problem, we can represent the total number of candidate design points in $\hat{\Omega}_f$ that belong to Ω_s as $\hat{S}_f$, and the total number of candidate design points in $\hat{\Omega}_s$ that belong to Ω_f as $\hat{S}_s$. The N_f is determined by:

$$N_f = \hat{N}_f + \hat{S}_s - \hat{S}_f \tag{22}$$

With a confidence level of α, the confidence interval of N_f can be expressed as follows:

$$N_f = \left[\hat{N}_f - \hat{S}_f^u,\ \hat{N}_f + \hat{S}_s^u \right] \tag{23}$$

where $\hat{S}^u$ and $\hat{S}_s^u$ are the upper bound of the confidence interval of $\hat{S}_s$ and $\hat{S}_f$, respectively.

The maximum error can be obtained by:

$$\varepsilon = \left| \frac{\hat{N}_f}{N_f} - 1 \right| \le max\left(\left| \frac{\hat{N}_f}{\hat{N}_f - \hat{S}_f^u} - 1 \right|,\ \left| \frac{\hat{N}_f}{\hat{N}_f + \hat{S}_s^u} - 1 \right| \right) = \hat{\varepsilon}_{max} \tag{24}$$

Since the distributions of $\hat{S}_s$ and $\hat{S}_f$ converge to the normal and Poisson distributions, respectively,

their upper bounds can be computed analytically. Adaptive reliability analysis stops when the following criterion is satisfied.

$$\hat{\varepsilon}_{max} \le \hat{\varepsilon}_{thr} \tag{25}$$

where $\hat{\varepsilon}_{thr}$ is a given error threshold.

4 Implementation procedure of the established method

Figure 8 depicts the flowchart illustrating the implementation process of the established method. The steps for assessing the reliability under uncertainties during freight wagon passing through the railway turnout are described as follows:

Step 1: Develop a freight wagon-turnout coupled dynamic simulation model and determine the statistical features of random parameters for the freight wagon and turnout structure.

Step 2: Generate N_0 initial samples ξ_{ini} by Latin hypercube sampling method. Calculate the corresponding dynamic responses of WRCFs P and Q through executing the command in the MATLAB environment for calling freight wagon turnout dynamic interaction model.

Step 3: Construct Kriging surrogate models for $g_i(\boldsymbol{\xi})$ with deterministic derailment criteria and $\tilde{g}_i(\boldsymbol{\xi})$ with random derailment criteria based on initial DoE and outputs in Step 2.

Step 4: Obtain prediction results by Kriging model. Then, evaluate the failure probability with different performance functions based on.

$$\hat{P}_f = \frac{\hat{N}_f}{N_{MCS}} \tag{26}$$

Step 5: Update the next best training sample point based on the active learning function in Equation (18). Calculate the corresponding dynamic responses of WRCF and obtain the maximum derailment coefficient and WLRR based on the freight wagon-turnout coupled dynamic interaction model.

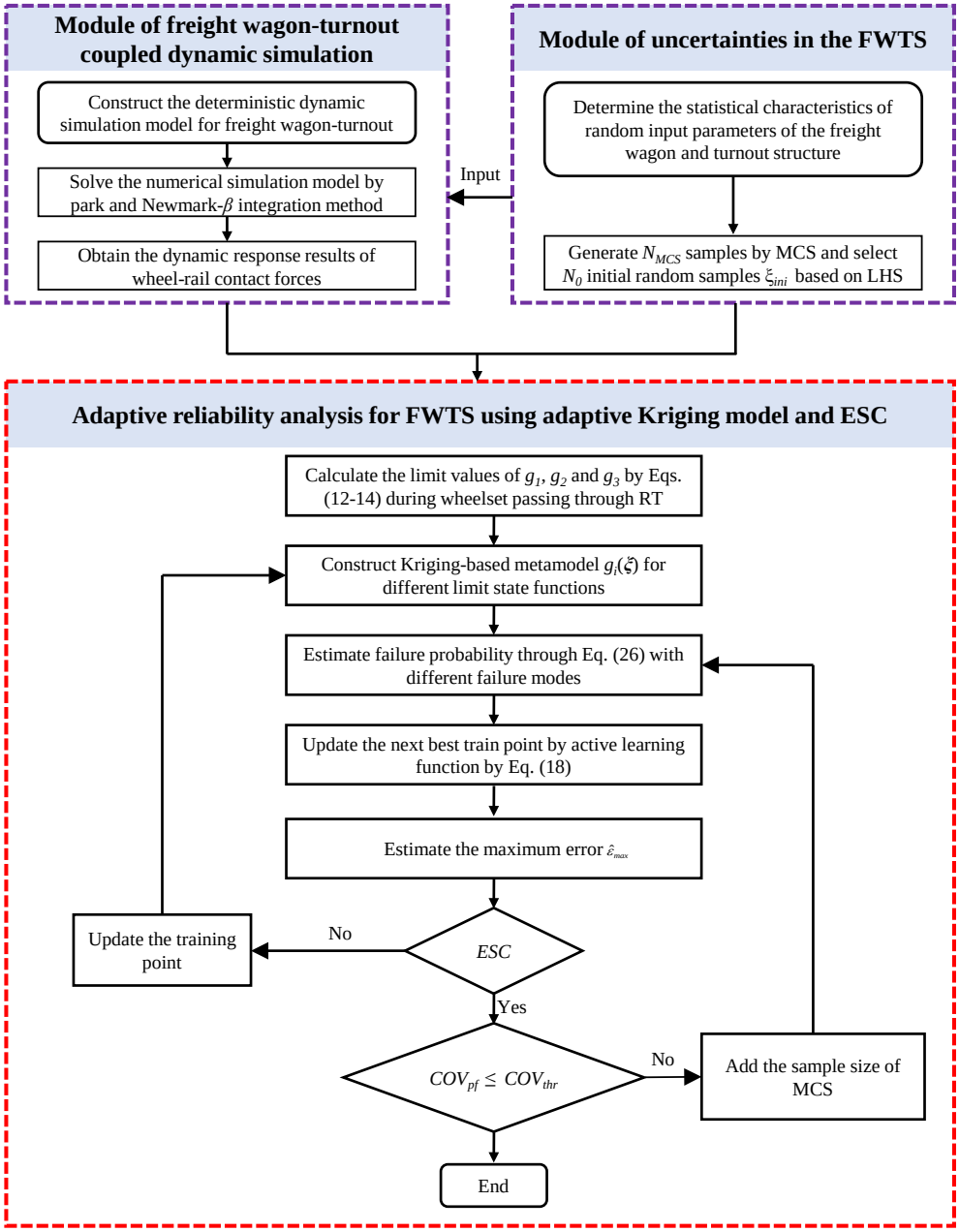

Figure 8. The flowchart of reliability analysis for derailment using freight wagon-turnout dynamic simulation and ESC-based active learning Kriging surrogate model.

Step 6: Compute the estimation error of reliability analysis using Equation (24), and verify whether ESC is met as indicated by Equation (25). If the stopping condition is satisfied, the adaptive iteration process ends. Instead, the current sample set is expanded with new samples until the stopping condition is satisfied.

Step 7: Evaluate the size of the initial Monte Carlo sample pool. Estimate the $COV_{\hat{P}_f}$ based on Equation

(27).

$$COV_{\hat{P}_f} = \sqrt{\frac{1-\hat{P}_f}{\hat{P}_f N_{MCS}}} \tag{27}$$

5 Results and discussion

5.1 Reliability assessment using deterministic derailment criteria

In this paper, the wheel derailment is considered as the failure event. Based on the simulation results obtain from the deterministic numerical analysis of the freight wagon-turnout dynamic model, the dynamic responses of the lateral and vertical WRCF, which represent the derailment risk at RT can be obtained. It should be noted that 20 initial samples are selected to construct the Kriging based surrogate model. Then, the reliability assessment for the freight wagon-turnout dynamic system is carried out by using the adaptive Kriging model and ESC.

The derailment coefficient is used to evaluate the wheel climb derailment caused by large lateral WRCF. In contrast, WLRR is used to assess wheel jump derailment when the wheel load on the railhead is suddenly reduced or disappeared. According to the Chinese railway standard TB/T2360-93, a freight wagon is deemed unsafe if the derailment coefficient limit λ exceeds 1.2 or the dynamic WLRR limit γ exceeds 0.80. Figure 9 (a-c) illustrate the convergence curves of failure probability when using different derailment criteria. In addition, the results using different error thresholds of 0.03, 0.04, and 0.05 are also compared.

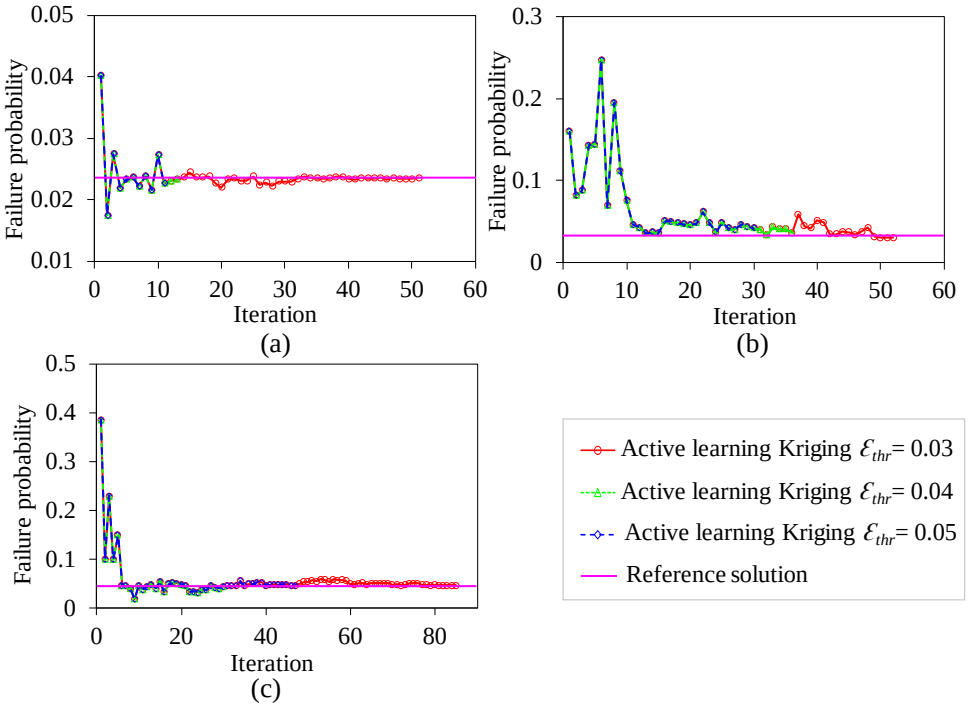

Figure 9. The failure probability using deterministic derailment criteria: (a) case 1: $g_1(\boldsymbol{\xi})$ (b) case 2: $g_2(\boldsymbol{\xi})$, and (c) case 3: $g_3(\boldsymbol{\xi})$.

The estimated failure probabilities of wheel climb derailment, wheel jump derailment, and both types of derailments with error threshold of 0.03, 0.04 and 0.05 are listed as **Table 3** The results in Figure 9 and **Table 3** show that the number of simulations of the freight wagon-turnout dynamic model for case 1 and case 3 increases significantly as the error threshold is reduced to 0.03. When compared with three performance functions, it shows that the failure probability of wheel jump derailment of case 2 is higher than that of wheel climb derailment. This is mainly due to the wheel impact on the switch rail when the freight wagon passes the switch toe; at the same time, the wheel load transition between the stock rail and the switch rail will lead to a direct and intense impact on the wheel, which in turn leads to a reduction in wheel load. The failure probability of P_{f3} is 0.2259, which is smaller than the sum of P_{f1} and P_{f2}. This indicates that in some running cases both the derailment coefficient and WLRR exceed the limit value.

To validate the feasibility of the proposed research framework, the reliability of freight wagon passing over the a #1:6 symmetrical is analyzed by using the ESC-based adaptive Kriging model. Since the computational cost of each call to the performance function takes several hours, the results of the Kriging model including 500 sets samples instead of the conventional MCS are considered as the reference solution.

When compared with the ESC-based adaptive Kriging method and Kriging method with N_{call}=500, the

errors in the failure probabilities obtained by the two methods are quite small when different performance functions are used to assess the running reliability. The proposed method yields precise failure probability of wheel derailment while significantly reducing the number of additional training points required and computation time. This is particularly advantageous for large-scale vibration system involving multiple failure modes and randomized failure domains, as encountered in this study.

Based on random inputs and reliability calculation results, as the wheel-rail friction coefficient and the lateral deviation of center of gravity position increase, the failure probability of wheel climb derailment at railway turnout increases significantly. For wheel jump derailment, the vehicle speed, wheelset axle load, and position of center of gravity have great influence on the failure probability related to wheel load loss.

Table 3. Comparison of computation efficiency and failure probability under different thresholds

Performance functions	Stopping criteria	N_{call}	P_f	$\hat{\varepsilon}_{max}$
$g_1(\xi)$	ESC ($\hat{\varepsilon}_{thr}$= 0.03)	20+51	0.0235	0.0293
	ESC ($\hat{\varepsilon}_{thr}$= 0.04)	20+13	0.0233	0.0382
	ESC ($\hat{\varepsilon}_{thr}$= 0.05)	20+11	0.0226	0.0458
	$U_{min}\geq 2$	20+145	0.0230	/
$g_2(\xi)$	ESC ($\hat{\varepsilon}_{thr}$= 0.03)	20+52	0.0301	0.0290
	ESC ($\hat{\varepsilon}_{thr}$= 0.04)	20+36	0.0364	0.0381
	ESC ($\hat{\varepsilon}_{thr}$= 0.05)	20+30	0.0392	0.0468
	$U_{min}\geq 2$	20+201	0.0322	/
$g_3(\xi)$	ESC ($\hat{\varepsilon}_{thr}$= 0.03)	20+87	0.0446	0.0292
	ESC ($\hat{\varepsilon}_{thr}$= 0.04)	20+40	0.0462	0.0387
	ESC ($\hat{\varepsilon}_{thr}$= 0.05)	20+30	0.0475	0.0485
	$U_{min}\geq 2$	20+232	0.0468	/

5.2 Reliability assessment using uncertain derailment criteria

Sometimes when the derailment coefficient or WLRR exceeds its limit value, the freight wagon does not necessarily derail. This paper is the first attempt to explore the impact of derailment criteria uncertainty on the running safety of railway vehicles. Since we now lack statistical characteristics of the derailment coefficient and WLRR when the vehicle derails in the turnout area. It is assumed that the derailment coefficient limit obeys a normal distribution, and the mean value and COV are 1.2 and 0.05, respectively. The WLRR obeys the uniform distribution and the upper limit and lower limit are 1.0 and 0.65. Figure 9 (a-c) show the convergence curves of failure probability with different evaluation criteria considering derailment criteria.

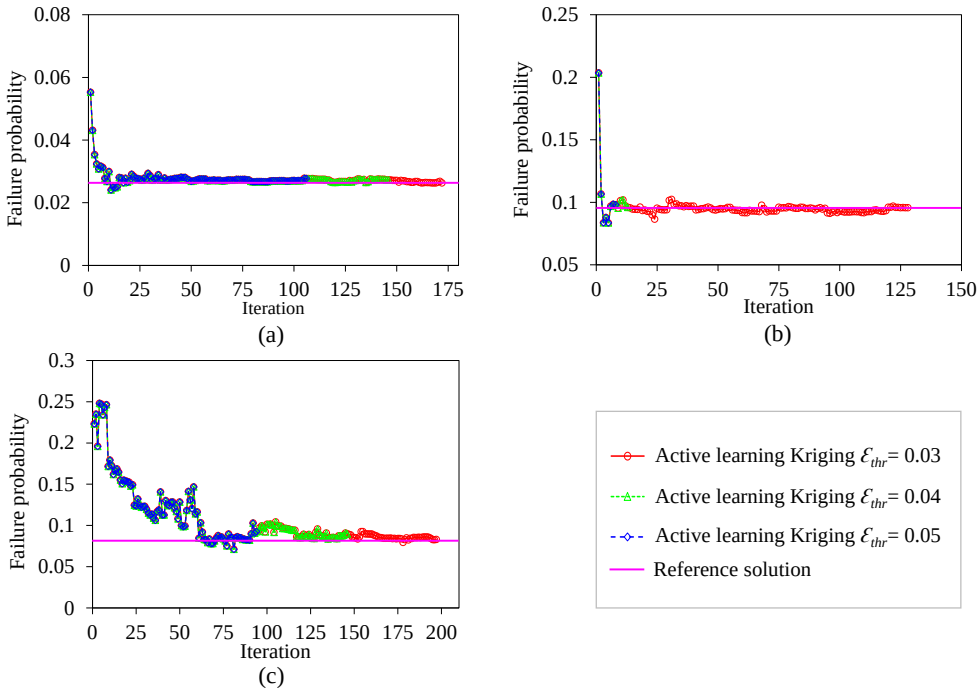

Figure 10. The failure probability using uncertain derailment criteria: (a) case 1: $\tilde{g}_1(\xi)$ (b) case 2: $\tilde{g}_2(\xi)$, and (c) case 3: $\tilde{g}_3(\xi)$.

When compared with the deterministic derailment coefficient, the failure probability of wheel climb derailment is lower than the result that is simulated by the deterministic derailment coefficient. This observation suggests that from a probabilistic standpoint, freight wagon derailment may occur even if the limit of the derailment coefficient is not exceeded. For example, there are instances where the wheel suddenly jumps on the rail despite the presence of relatively small lateral WRCF. However, the failure probability of wheel jump derailment, when accounting for the uncertainty of the WLRR, is lower than the deterministic limit value. This is because the randomness of the WLRR is considered in this section and the freight wagon is still safe when the WLRR exceeds 0.65. **Table 4** lists the main reliability analysis results when the uncertainty of the derailment criteria is considered. It can be seen from the results in Figure 10 that the failure probabilities calculated by ESC-based adaptive Kriging are more consistent with the results calculated by Kriging with N_{call}=500.

Table 4. Comparison of computation efficiency and failure probability under different failure modes.

Performance functions	Stopping criteria	N_{call}	P_f	$\hat{\varepsilon}_{max}$
$\tilde{g}_1(\xi)$	ESC ($\hat{\varepsilon}_{thr}$= 0.03)	20+172	0.0263	0.0282
	ESC ($\hat{\varepsilon}_{thr}$= 0.04)	20+145	0.0274	0.0393
	ESC ($\hat{\varepsilon}_{thr}$= 0.05)	20+105	0.0271	0.0475
	$U_{min}\geq 2$	20+252	0.0268	/
	ESC ($\hat{\varepsilon}_{thr}$= 0.03)	20+128	0.0956	0.0295

$\tilde{g}_2(\xi)$	ESC ($\hat{\varepsilon}_{thr}$= 0.04)	20+12	0.0959	0.0399
	ESC ($\hat{\varepsilon}_{thr}$= 0.05)	20+8	0.0984	0.0494
	U_{min}≥2	20+292	0.0971	/
$\tilde{g}_3(\xi)$	ESC ($\hat{\varepsilon}_{thr}$= 0.03)	20+197	0.0830	0.0299
	ESC ($\hat{\varepsilon}_{thr}$= 0.04)	20+145	0.0909	0.0397
	ESC ($\hat{\varepsilon}_{thr}$= 0.05)	20+93	0.0907	0.0495
	U_{min}≥2	20+402	0.0916	/

5.3 Reliability analysis considering rail wear evolution of the turnout

To further verify the applicability of the research framework proposed in this study, the effect of rail wear evolution on the reliability of the FWTS was investigated. As the density of freight wagons is becoming more and more intensive, which leads to the increasingly prominent problem of rail wear at the turnouts. Rail wear would directly affect the running performance when the railway vehicle passes through the turnout. In this paper, the evolution of the rail profile of a new turnout with the change of operation time was tracked and tested, as shown in Figure 11.

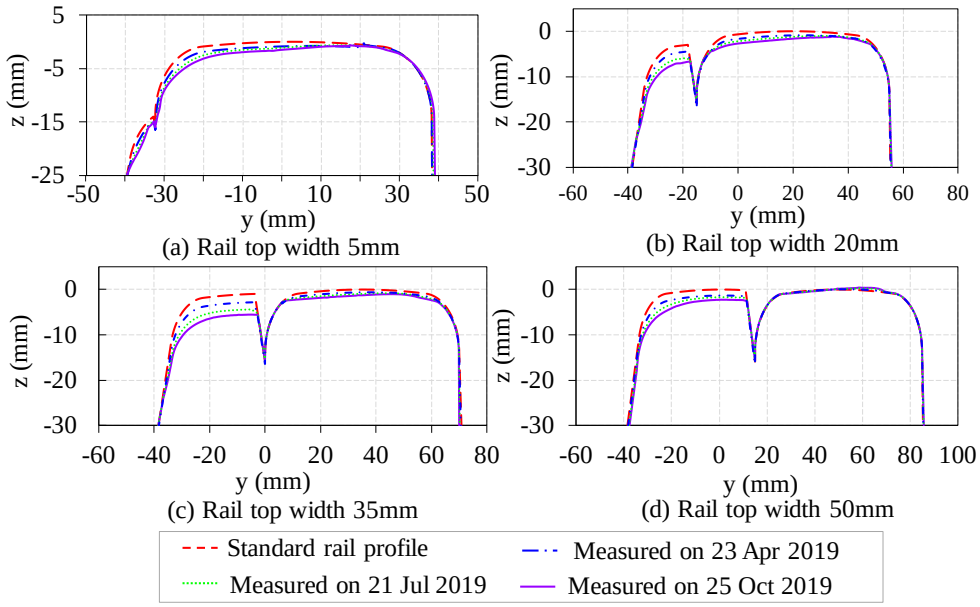

Figure 11. Measured rail profiles of the switch panel.

The relationship between the derailment coefficient and failure probability P_{f1} and the relationship between WLRR and failure probability P_{f2} with the evolution of the rail wear are depicted in Figure 12(a) and (b). As can be seen from Figure 12, the failure probability of the FWTS increases with increasing derailment coefficient and WLRR for the rail profiles measured in different periods. The rail wear evolution has a significant impact on the failure probability of wheel climb derailment, as depicted in Figure 12(a). Under the same derailment criteria, the failure probability shows a positive correlation with the depth of rail wear, indicating that the safety of the freight wagon decreases with an increase in rail wear depth. The

relationship between the derailment criteria and the failure probability under different degrees of rail wear provides valuable insights for safety improvement and structural optimization design, applicable to both railway vehicles and turnouts.

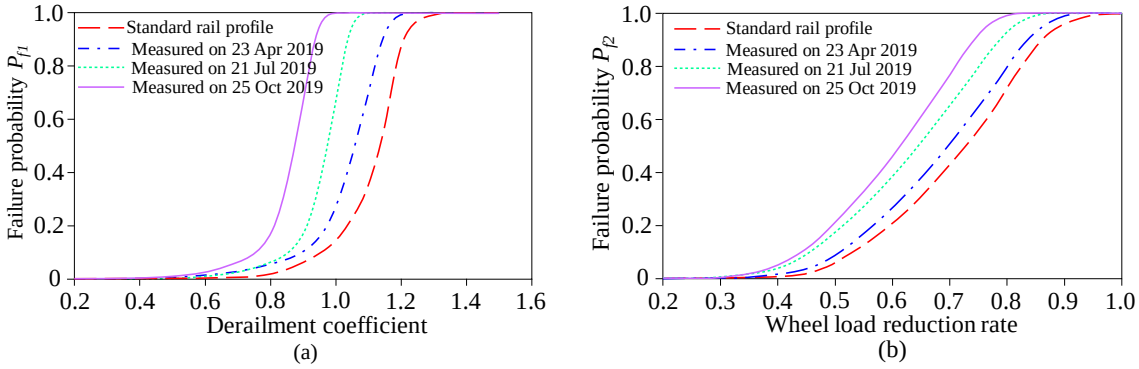

Figure 12. (a) Relationship between derailment coefficient and failure probability and (b) relationship between WLRR and failure probability.

6 Conclusions

This paper presents an efficient active learning Kriging method to assess the safety and reliability of railway vehicle passing through railway turnouts when considering the nonlinear dynamic interactions between the vehicle and turnout. The influence of multiple sources of uncertainty, including turnout geometry uncertainty, vehicle suspension parameter variations and load variations, on the multiple failure modes of derailment is investigated. The main conclusions of this study are summarized as follows:

1. The freight wagon-turnout coupled dynamic model that considers the multi-point contact situation between the wheels and turnout has been developed in detail. A field test was carried out to verify the vehicle-turnout dynamic interaction model. The simulation results are in good agreement with the field test data.
2. Based on the adaptive reliability analysis framework for the FWTS, the derailment probabilities under multiple failure modes of wheel derailment are evaluated. The results indicate that the failure probability of wheel jump derailment caused by wheel load loss is higher than that of wheel climb derailment under large lateral wheel-rail force. This is mainly attributed to the presence of discontinuous tracks in the turnout area, which result in significant impacts on the wheels during the wheel-rail transition. Additionally, the presence of small radius curves before the turnout causes the wheelset to enter the turnout in an unfavourable posture, further leading to collisions with the switch rail.

3. This paper explores for the first time the influence of uncertain derailment criteria on the reliability of train derailment. When the randomness of the derailment coefficient limit is considered, it shows that the safety level might be underestimated by using the deterministic derailment coefficient to assess the running safety. In contrast, when the wheel load reduction ratio follows a uniform distribution between 0.65 and 1, the probability of failure is lower when compared with the results calculated by deterministic limit. It can be concluded that it is necessary to consider the randomness of the derailment limit value when assessing the reliability of FWTS.
4. The proposed approach is extended to assess the effect of the rail wear evolution on running reliability of the freight wagon. The results show that as the wear depth of the turnout rails increases, the probability of both wheel climb derailment and wheel jump derailment of the freight wagon increases. The risk of wheel climb derailment increases more significantly. The relationship between derailment index and derailment probability under different rail wear states has important guiding significance for the engineering application of turnout rail grinding.
5. The adaptive Kriging model shows efficient and highly accurate approximation capability in dealing with the nonlinear contact between the wheel and the turnout. The convergence process of the reliability analysis for the stopping criterion $U_{min}\geq 2$ and ESC ($\hat{\varepsilon}_{thr}$ =0.05) is compared, and the results indicate that fewer iterations are required to achieve the desired accuracy when ESC is used as the stopping criteria. This approach provides valuable insight into the structural design and optimization of railway vehicles and turnouts.
6. The research framework and corresponding codes developed in this study can be easily extended to the safety assessment of other weak parts of the track structure, such as sharp curves, rail joints, transition sections of subgrade.

Declaration of Competing Interest

The authors declared that there is no conflict of interest.

Acknowledgments

The work was supported by National Natural Science Foundation of China (Grant No. 52122810 and 52108418), and Natural Science Foundation of Sichuan Province, China (Grant No. 2023NSFSC0398).

References

[1] Sysyn M, Gerber U, Kluge F, et al. Turnout remaining useful life prognosis by means of on-board inertial

measurements on operational trains. International Journal of Rail Transportation, 2020, 8(4): 347-369.

[2] Dindar S, Kaewunruen S, An M, et al. Bayesian Network-based probability analysis of train derailments caused by various extreme weather patterns on railway turnouts. Safety science, 2018, 110: 20-30.

[3] Liu X, Saat MR, Barkan CPL. Analysis of causes of major train derailment and their effect on accident rates. Transportation Research Record, 2012, 2289(1): 154-163.

[4] Kassa E, Nielsen JCO. Dynamic train–turnout interaction in an extended frequency range using a detailed model of track dynamics. Journal of sound and vibration, 2009, 320(4-5): 893-914.

[5] Bruni S, Anastasopoulos I, Alfi S, et al. Effects of train impacts on urban turnouts: Modelling and validation through measurements. Journal of Sound and Vibration, 2009, 324(3-5): 666-689.

[6] Chang C, Ding X, Ling L, et al. Mechanism of high-speed train carbody shaking due to degradation of wheel-rail contact geometry. International Journal of Rail Transportation, 2023, 11(3): 289-316.

[7] Xu L, Liu X. Matrix coupled model for the vehicle–track interaction analysis featured to the railway crossing. Mechanical Systems and Signal Processing, 2021, 152: 107485.

[8] Chen J, Wang P, Xu J, et al. Simulation of vehicle-turnout coupled dynamics considering the flexibility of wheelsets and turnouts. Vehicle System Dynamics, 2023, 61(3): 739-764.

[9] Chen R, Chen J, Wang P, et al. Impact of wheel profile evolution on wheel-rail dynamic interaction and surface initiated rolling contact fatigue in turnouts. Wear, 2019, 438: 203109.

[10] Lai J, Xu J, Wang P, et al. Numerical investigation of dynamic derailment behavior of railway vehicle when passing through a turnout. Engineering Failure Analysis, 2021, 121: 105132.

[11] Lai J, Xu J, Wang P, et al. Numerical investigation on the dynamic behaviour of derailed railway vehicles protected by guard rail. Vehicle system dynamics, 2021, 59(12): 1803-1824.

[12] Lai J, Xu J, Liao T, et al. Investigation on train dynamic derailment in railway turnouts caused by track failure. Engineering Failure Analysis, 2022, 134: 106050.

[13] Tong F, Gao L, Hou B, et al. Influence of differential deterioration of random track irregularity at different wavelengths on high-speed train safety. International Journal of Rail Transportation, 2023: 1-23.

[14] Wang S, Luo J, Zhu S, et al. Random dynamic analysis on a high-speed train moving over a long-span cable-stayed bridge. International Journal of Rail Transportation, 2022, 10(3): 331-351.

[15] Karamchandani A, Cornell CA. Sensitivity estimation within first and second order reliability methods. Structural Safety, 1992, 11(2): 95-107.

[16] Shinozuka M. Basic analysis of structural safety. Journal of Structural Engineering, 1983, 109(3): 721-740.

[17] Kaymaz I, McMahon CA. A response surface method based on weighted regression for structural reliability analysis. Probabilistic Engineering Mechanics, 2005, 20(1): 11-17.

[18] Li J. Probability density evolution method: background, significance and recent developments. Probabilistic Engineering Mechanics, 2016, 44: 111-117.

[19] Teixeira R, Nogal M, O'Connor A. Adaptive approaches in metamodel-based reliability analysis: A review. Structural Safety, 2021, 89: 102019.

[20] Li Z, Zhou Y, Liu X, et al. Service reliability assessment of ballastless track in high speed railway via improved response surface method. Reliability Engineering & System Safety, 2023, 234: 109180.

[21] Wang W, Zhang Y, Ouyang H. Modeling uncertainties of vehicle-track coupled dynamic systems. Mechanics Based Design of Structures and Machines, 2021, 49(7): 947-968.

[22] Xu L, Zhai W. Stochastic analysis model for vehicle-track coupled systems subject to earthquakes and track random irregularities. Journal of Sound and Vibration, 2017, 407: 209-225.

[23] Ma X, Zhang Z, Hua H. Uncertainty quantization and reliability analysis for rotor/stator rub-impact using advanced Kriging surrogate model. Journal of Sound and Vibration, 2022, 525: 116800.

[24] Cremona MA, Liu B, Hu Y, et al. Predicting railway wheel wear under uncertainty of wear coefficient, using universal kriging. Reliability Engineering & System Safety, 2016, 154: 49-59.

[25] Costa JN, Ambrósio J, Andrade AR, et al. Safety assessment using computer experiments and surrogate modeling: Railway vehicle safety and track quality indices. Reliability Engineering & System Safety, 2023, 229: 108856.

[26] Bichon BJ, Eldred MS, Swiler LP, et al. Efficient global reliability analysis for nonlinear implicit performance functions. AIAA journal, 2008, 46(10): 2459-2468.

[27] Echard B, Gayton N, Lemaire M. AK-MCS: an active learning reliability method combining Kriging and Monte Carlo simulation. Structural Safety, 2011, 33(2): 145-154.

[28] Peijuan Z, Ming WC, Zhouhong Z, et al. A new active learning method based on the learning function U of the AK-MCS reliability analysis method. Engineering structures, 2017, 148: 185-194.

[29] Shi Y, Lu Z, He R, et al. A novel learning function based on Kriging for reliability analysis. Reliability Engineering & System Safety, 2020, 198: 106857.

[30] Zhai W, Wang K, Cai C. Fundamentals of vehicle–track coupled dynamics. Vehicle System Dynamics, 2009, 47(11): 1349-1376.

[31] Zhai W. Vehicle–track coupled dynamics: Theory and applications. Springer Singapore, 2020.

[32] Xu J, Wang P, Wang L, et al. Effects of profile wear on wheel–rail contact conditions and dynamic interaction of vehicle and turnout. Advances in mechanical Engineering, 2016, 8(1): 1-14.

[33] Wang Z, Shafieezadeh A. ESC: an efficient error-based stopping criterion for kriging-based reliability analysis methods. Structural and Multidisciplinary Optimization, 2019, 59: 1621-1637.